# LES of a high Reynolds, high subsonic jet : effects of the subgrid modellings on flow and noise.*

Christophe Bogey† and Christophe Bailly‡

Laboratoire de Mécanique des Fluides et d'Acoustique
Ecole Centrale de Lyon & UMR CNRS 5509
69134 Ecully, France.

## Abstract

Large Eddy Simulations (LES) of a Mach number M = 0.9, round jet with a high Reynolds number $Re_D = 4 \times 10^5$ are performed. In first LES, a selective filtering removing grid-to-grid oscillations without affecting the resolved scales is used alone to take into account the dissipative effects of the unresolved scales. Flow and noise are shown to be independent on the filtering. In second LES, the dynamic Smagorinsky eddy-viscosity model (DSM) is also applied. Results are found not to be appreciably modified when a subgrid scale kinetic energy is combined with the DSM. Moreover, the flow features differ significantly using the DSM or using the filtering alone. Using the DSM, the jet develops faster with higher turbulence intensities and larger length scales, and the high-frequency components in the velocity and sound spectra are reduced. This supports that the effective Reynolds number of the simulated flow is artificially decreased by the use of an eddy viscosity.

## 1. Introduction

Solving the Navier-Stokes equations for simulating turbulent flows raises important issues which need to be addressed to ensure that the solutions are physically correct and are not artifacts of the computational procedure. This is particularly the case for the numerical dissipation, whose effects are to be minimized so that they do not exceed the physical mechanisms nor do govern the flows. For instance in Direct Numerical Simulation (DNS) where all the turbulent scales down to the energy-dissipating scales are solved, one must check that the molecular viscosity dominates the numerical dissipation. In Large Eddy Simulation (LES) where only the turbulent scales discretized by the grid are calculated, this point is quite different since the scales affected by viscous diffusion are lacking. An artificial damping is then required to dissipate the turbulent kinetic energy, and in practice to ensure stability.

The usual LES approach to account for the dissipative effects of the subgrid scales rests on an eddy-viscosity hypothesis.[1] Models such as the famous Smagorinsky model[2] have thus been developed to express the eddy viscosity from physical considerations. They have been improved by the formulation of dynamic procedures[3–5] to estimate the coefficient adjusting the amplitude of the eddy viscosity directly from the computed scales. These procedures are based on the use of the eddy-viscosity model twice, to represent the subgrid stress tensors associated, respectively, to the grid filter and to an arbitrary test filter of larger width. The major benefit using dynamic procedures is that the eddy viscosity should vanish for laminar flow. However the eddy-viscosity approach still suffers from several deficiencies. The eddy-viscosity closure assumes a one-to-one correlation between the subgrid stress and the resolved strain rate tensors although very little correlation really exists.[6] The dynamic procedures are also quite sensitive to the numerical errors[7] and to the shapes of the test filters.[8] Despite these limitations, the eddy-viscosity models are widely used, notably in combination with other parametrizations of the subgrid stress tensor[1,9,10] in mixed models.

One important question raised by an eddy-viscosity model is about the effective Reynolds number of the simulated flows.[11,12] Since the eddy and the molecular viscosities have the same functional form, one can expect an eddy viscosity of higher amplitude than the molecular viscosity to define the effective flow Reynolds number. Its value might thus be artificially decreased. Moreover, an eddy viscosity may dissipate the turbulent energy through a



†Research scientist CNRS, christophe.bogey@ec-lyon.fr

‡Assistant Professor, Member AIAA, christophe.bailly@ec-lyon.fr

wide range of scales up the larger which should be dissipation-free. Alternatives to the eddy-viscosity models have therefore been proposed.[13] One interesting approach consists in damping the turbulent energy by numerical procedures.[14] To closely control the numerical dissipation, it appears especially appropriate to use compact[15,16] or selective[17] filters whose properties are optimized in the wave number space to eliminate short waves without affecting the resolved scales. The use of compact filtering without additional subgrid model was recently tested by Visbal and Rizetta[18] who obtained better results using compact filtering alone than with Smagorinsky models for isotropic turbulence. In an earlier work, selective filtering was also chosen by the authors to take into account the dissipative effects of the unresolved scales with the aim of performing Reynolds-Number-Preserving LES. The circular jet thus simulated displayed properties in good agreement with relevant measurements.[11]

In the present paper, LES of the same jet with a Mach number M = 0.9 and a Reynolds number $\mathrm{Re}_D = 4 \times 10^5$ are presented to study the influence of the subgrid modelling on jet flow and noise, which are expected to be significant at such a high $\mathrm{Re}_D$. Two kinds of simulations are carried out using selective filtering alone or in combination with the Dynamic Smagorinsky Model (DSM). To ensure that the scales involved in the dynamic procedure are well calculated, the numerical solver displays spectral-like accuracy, providing negligible dissipation and dispersion on the resolved scales. The first object of this work is to demonstrate that the flow solution is independent on the filtering when filters used are sufficiently selective. The second is to show the possible effects of the addition in the DSM simulations of a scale subgrid kinetic energy, usually proposed as modelling for the isotropic part of the subgrid stress tensor.[19] The third and main object is to compare the results obtained with and without the DSM, to investigate the influence of an eddy viscosity model on the turbulent jet features, and especially on the effective flow Reynolds number. Note that the role of the eddy viscosity will be further discussed in a next paper[20] from the kinetic energy balance.

The numerical procedure is presented and the different simulations are defined in section 2, displaying also snapshots of vorticity and pressure. The influence on results of the selective filtering and this of the subgrid scale kinetic energy in the DSM simulations are shown in sections 3 and 4, respectively. The flow and sound fields obtained with the filtering alone and with the DSM are compared in section 5. Finally concluding remarks are drawn in section 6.

## 2. Simulation parameters

### 2.1 Numerical procedure

The numerical algorithm is this of earlier simulations[11,21] of the present isothermal round jet at M = 0.9 and $\mathrm{Re}_D = 4 \times 10^5$. The filtered compressible Navier-Stokes equations[22] are solved using low dispersive and low dissipative schemes.[17] A thirteen-point finite-difference scheme is used for spatial discretization while an explicit six-stage Runge-Kutta algorithm is applied for time integration. For stability, grid-to-grid oscillations are removed thanks to a selective filtering reported in the next subsection. To compute the noise, non-reflective boundary conditions as well as a sponge zone at the outflow[23] are implemented.

The inflow conditions and the numerical parameters of the simulations are those of the simulation referred to as LESac in earlier papers.[11,21] Meanflow profiles are imposed at the inflow boundary with a ratio between the shear-layer momentum thickness and the jet radius of $\delta_\theta / r_0 = 0.05$. Random disturbances are added to the velocity profiles in the shear layer zone to seed the turbulence.[24] The excitation procedure is described in detail in a recent paper[21] where the effects of the inflow conditions on flow and sound fields are studied for the present jet.

The computational domain is discretized by a 12.5 million point Cartesian grid with 15 points in the jet radius $r_0$. The flow is computed up to an axial distance of $25 r_0$. The sound field is calculated radially up to $15 r_0$ from the jet axis, and resolved for Strouhal numbers $St = fD/u_j < 2$. Finally, the simulation time $T$ is long enough to achieve convergence of results, as shown for instance by the corresponding Strouhal number $D/(Tu_j) = 9.9 \times 10^{-4}$.

### 2.2 Definition of the different simulations

In all simulations, an explicit filtering is applied to the density, momentum and pressure. The filters used[11] were designed to eliminate short waves without affecting the resolved scales discretized at least by four grid points. Their transfert functions can be found in references.[11,17] One can expect this selective filtering to act as the subgrid scales by dissipating the turbulent energy transferred from the resolved scales.

To define the LES, remind that the application of a central, $2N+1$ point stencil filter to a variable $U$, on a mesh of spacing $\Delta x$, is performed as

$$U^f(x_0) = U(x_0) - \sigma_d \sum_{j=-N}^{N} d_j U(x_0 + j\Delta x)$$

where $0 \leq \sigma_d \leq 1$ and $d_j$ are the filter coefficients. Four simulations are carried out with the parameters reported in Table 1. Note that the simulation referred to as LESsf corresponds to the simulation LESac whose results have been presented previously.[11,17] In the simulations LESsf and LESsf2, the filtering is used alone without additional subgrid models, every two and three iterations respectively, with $\sigma_d = 2/3$.

| | *sf* every | $\sigma_d$ | $\nu_t$ | $k_{sgs}$ |
|---|---|---|---|---|
| LESsf | $2\Delta t$ | 2/3 | no | no |
| LESsf2 | $3\Delta t$ | 2/3 | no | no |
| LESdsm | $2\Delta t$ | 2/3 | yes | no |
| LESdsm2 | $2\Delta t$ | 2/3 | yes | yes |

Table 1: Parameters of the simulations, *sf* is used for *selective filtering*, $\Delta t$ is the time step.

In LESdsm and LESdsm2, the filtering is applied as in LESsf, but eddy viscosity $\nu_t$ and subgrid kinetic energy $k_{sgs}$ are also involved. The eddy viscosity and subgrid scale kinetic energy are used to approximate the deviatoric and isotropic parts of the subgrid stress tensor $\mathcal{T}_{ij}$, then expressed as

$$\mathcal{T}_{ij} = \overline{\rho}\widetilde{u}_i\widetilde{u}_j - \overline{\rho}\widetilde{u_i u_j} \simeq 2\mu_t \widetilde{S}^D_{ij} - 2\overline{\rho}k_{sgs}\delta_{ij}/3$$

where the superscript $D$ denote the deviatoric part, the bar and tilde indicate the LES filterings for compressible turbulence, see in Moin *et al.*[4] for more details. The eddy viscosity is parametrized using the Smagorinsky model as $\mu_t = \overline{\rho}C\Delta^2\widetilde{S}$, and the SGS kinetic energy as $k_{sgs} = C_I\Delta^2\widetilde{S}^2$ where $\Delta = (\Delta x\Delta y\Delta z)^{1/3}$ and $\widetilde{S} = (2\widetilde{S_{ij}}\widetilde{S_{ij}})^{1/2}$. The coefficients $C$ and $C_I$ are computed from a dynamic Germano-Lilly[4,5] procedure leading to

$$C = \left\langle L^D_{ij}M_{ij}\right\rangle / \left\langle M^2_{ij}\right\rangle \quad \text{and} \quad C_I = \langle L_{kk}\rangle / \langle N\rangle$$

where $\widehat{\ }$ represents a fifteen-point stencil test filter[17] of width $k_c\Delta x = \pi/2$, $\langle\ \rangle$ a second-order filter, and

$$\begin{cases} L_{ij} &= \widehat{\overline{\rho u_i}}\,\widehat{\overline{\rho u_j}}/\widehat{\overline{\rho}} - \widehat{[\overline{\rho u_i}\ \overline{\rho u_j}/\overline{\rho}]} \\ M_{ij} &= 2\widehat{\overline{\rho}}\widehat{\Delta}^2\breve{S}(\breve{S}_{ij} - \breve{S}_{kk}\delta_{ij}/3) \\ & \quad -\widehat{[2\overline{\rho}\Delta^2\widetilde{S}(\widetilde{S}_{ij} - \widetilde{S}_{kk}\delta_{ij}/3)]} \\ N &= -2\widehat{\overline{\rho}}\widehat{\Delta}^2\breve{S}^2 + \widehat{[2\overline{\rho}\Delta^2\widetilde{S}^2]} \end{cases}$$

with $\breve{\ }$ denoting test-filtered quantities.

Profiles for $r = r_0$ of the coefficients $C$ and $C_I$ obtained in LESdsm2 are presented in Figure 1. Although not shown, note that the coefficient $C$ takes very close values in LESdsm and LESdsm2. Its mean value of about 0.02 in the turbulent flow region stands in the range of values obtained for isotropic turbulence, from the Smagorinky constant yielding $C_s^2 = 0.18^2 = 0.032$, or from numerical simulations.[4,19,25] The mean value of $C_I$, about 0.01, corresponds also fairly well to the values calculated for isotropic turbulence.[4,25]

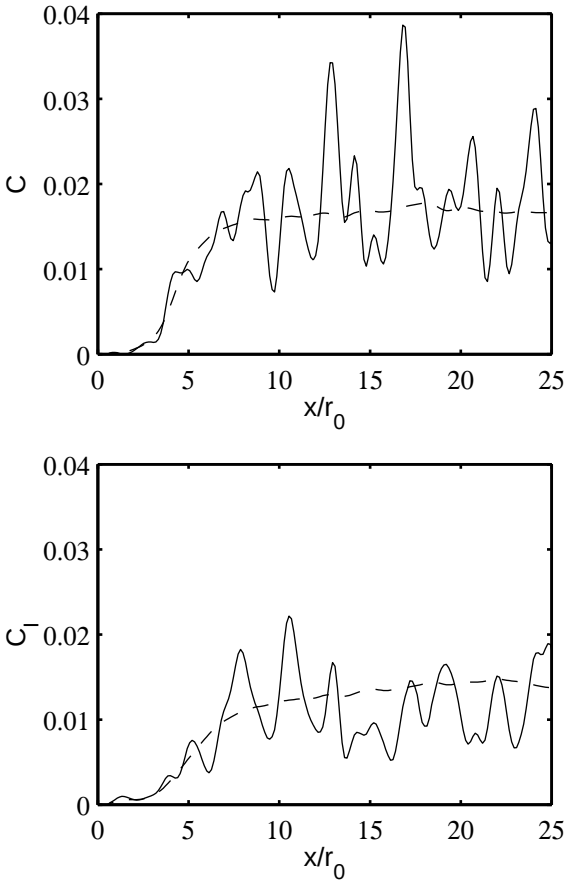


Figure 1: Profiles for $r = r_0$ of the dynamic coefficients $C$ and $C_I$ for the simulation LESdsm2: ——— instantaneous, and — — — time-averaged values.

In next sections, profiles plotted to compare the results obtained from the different simulations will follow the line type definition of Table 2.

| | |
|---|---|
| LESsf | ——— |
| LESsf2 | — · — · |
| LESdsm | — — — |
| LESdsm2 | ····· |

Table 2: Line types used for the four simulation profiles.

### 2.3 Instantaneous vorticity and pressure

Figures 2 and 3 present snapshots of the vorticity norm and of the fluctuating pressure for the simulations LESsf and LESdsm.

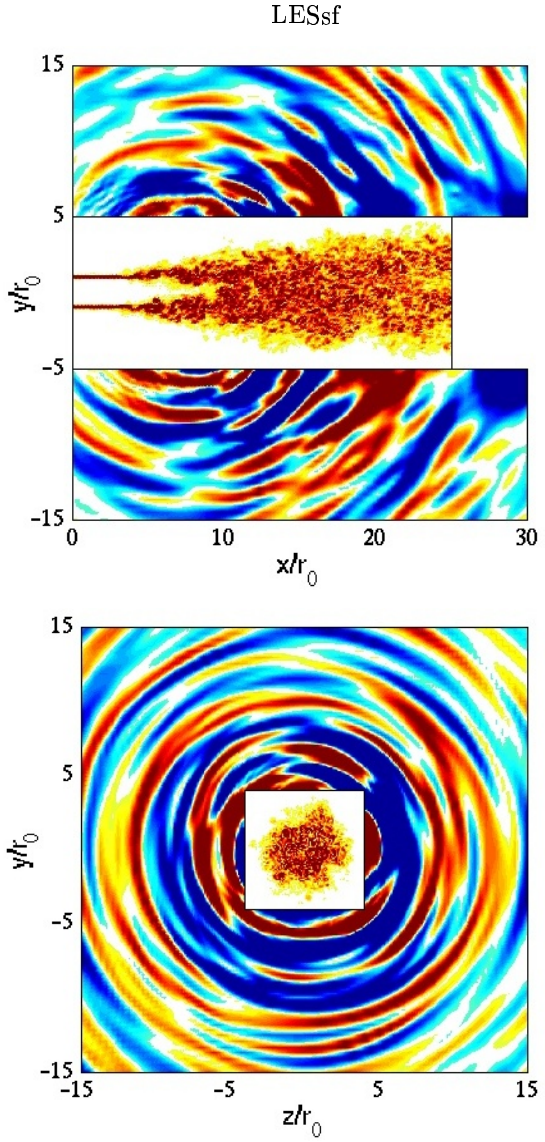


Figure 2: Snapshots of the vorticity $|\boldsymbol{\omega}|$ in the flow and of the fluctuating pressure $p'$ outside, for the simulation LESsf: in the $x-y$ plane at $z=0$ and in the $y-z$ plane at $x=11r_0$. The color scales are from 0 to $8\times10^4$ s$^{-1}$ for the vorticity and from $-70$ to 70 Pa for the pressure.

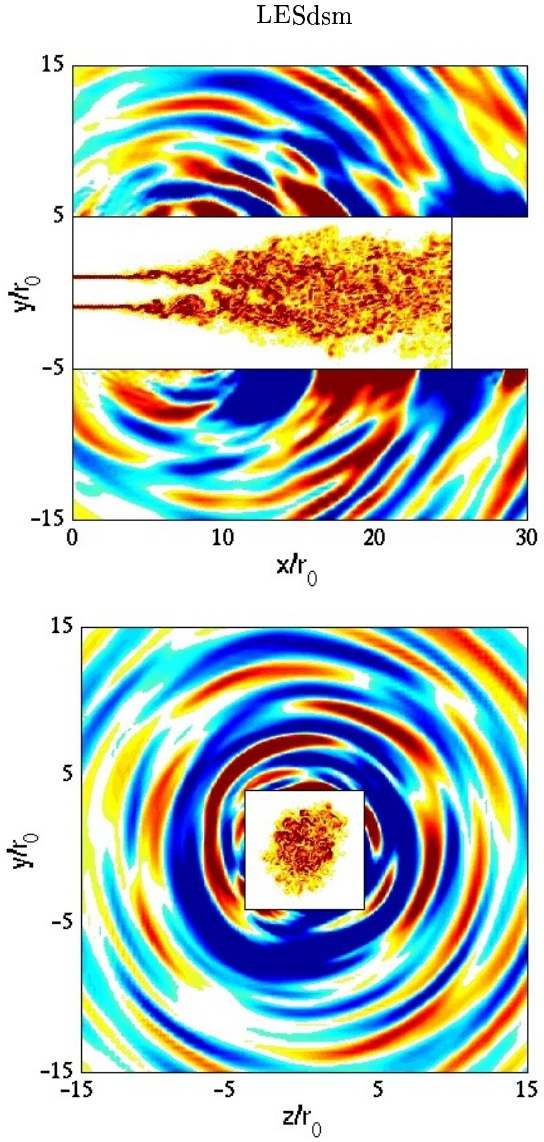


Figure 3: Snapshots of the vorticity and of the fluctuating pressure for the simulation LESdsm. See caption of Figure 2 for details.

The jet developments in LESsf and LESdsm look alike. They are characterized by core lengths $x_c$ of $10.2r_0$ and $10.4r_0$, respectively, determined here from the centerline mean axial velocities later shown in Figure 11 using $u_c(x_c) = 0.95u_j$. However it seems that the turbulent flow field displays more fine scales in LESsf, and that possible coherent structures are more apparent in LESdsm. A similar observation is made for the sound field, which contains visibly more high-frequency components in LESsf than in LESdsm as illustrated in the transverse planes, see in section 5 for detailed comparisons between the results from the two simulations.

### 3. Influence of the selective filtering

The sensitivity of LES results to the filtering should depend on the filter properties. Visbal and Rizetta[18] have for instance shown that low-order filters provide excessive dissipation for decaying isotropic turbulence and that at least 6th order is required to obtain correct results. Another example of the effects of filtering in LES is given by Uzun *et al.*[26] who reported that the features of a circular jet can vary according to the filters used.

In the present simulations, the filters are sufficiently selective so that the filtering exerts no influence on the resolved scales discretized by more than four grid points. The larger resolved scales, which are the major energy-containing scales and which thus determine the amount of energy to be dissipated, are unaffected. Therefore the dissipation rate, and consequently the LES results, should be independent on the filtering procedure. Physically, the turbulence spectra are truncated at the grid cut-off wave number $k_c^{grid} = \pi/\Delta x$, but accuratly calculated up to the filtering cut-off wave number here close to $k_c^{sf} = \pi/(2\Delta x)$. Energy is transferred, following the turbulent cascade process, from the resolved to the filtered scales characterized by $k > k_c^{sf}$, and is then diffused by the filtering.

The negligible influence of the selective filtering on the present LES results is demonstrated by the quite similar properties of the flow and sound fields obtained from the simulations LESsf and LESsf2 where the filtering is applied every two and three iterations respectively. Among the compared parameters, an excellent agreement is observed for the mean flow, the turbulence intensities, the velocity spectra and length scales, and for the sound levels and spectra, see for example Figures 4 and 5 displaying centerline profiles of the rms axial-velocity fluctuations and sideline acoustic levels.

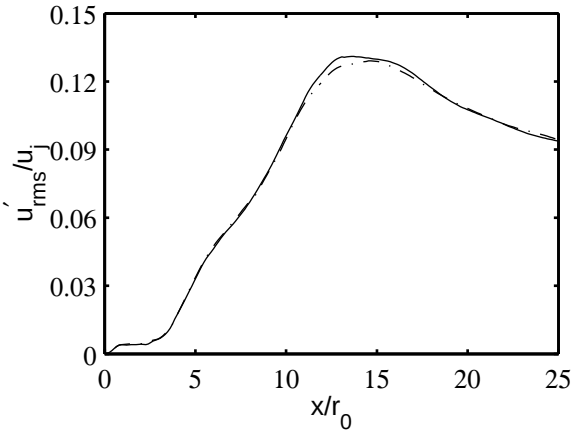


Figure 4: Centerline profiles of the rms-value of the fluctuating axial velocity. See Table 2 for the line types.

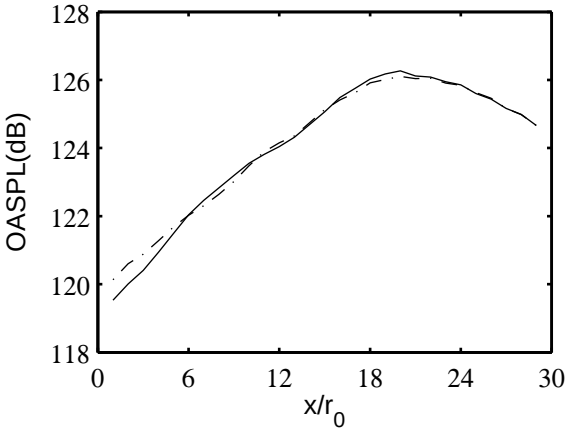


Figure 5: Overall sound pressure levels for $r = 15r_0$. See Table 2 for the line types.

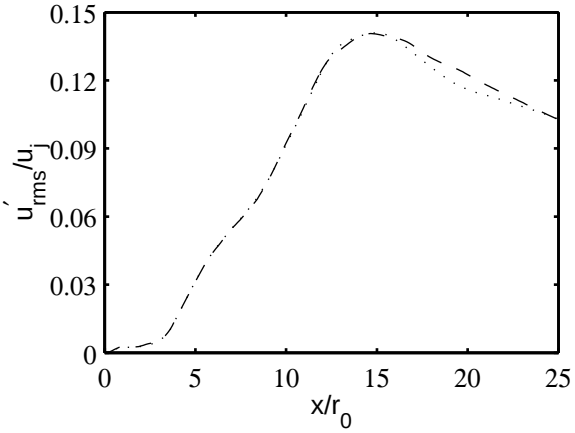


Figure 6: Centerline profiles of the rms-value of the fluctuating axial velocity. See Table 2 for the line types.

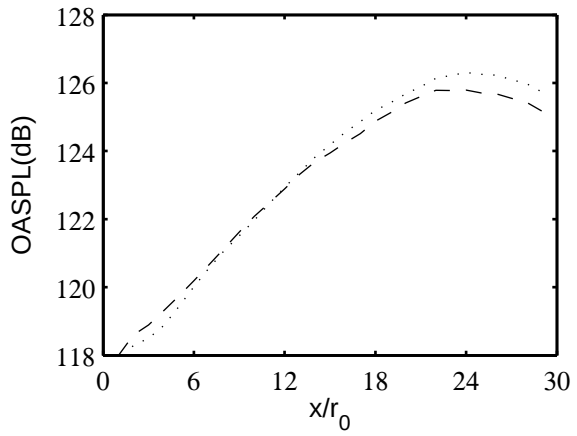


Figure 7: Overall sound pressure levels for $r = 15r_0$. See Table 2 for the line types.

## 4. Influence of the SGS kinetic energy

For compressible turbulence, eddy-viscosity models are usually combined with a model of the isotropic part of the SGS stress tensor based on SGS kinetic energy.[19] The physical justification of a SGS kinetic energy can be questioned by the mixing-layer simulations of Vreman *et al.*[22] where the small correlation between the SGS stress tensor and the dynamic Smagorinsky model was found to still decrease when a SGS kinetic energy is added. The effects of SGS kinetic energy are also very unclear. They were assumed to be negligible in most turbulent flows by Erlebacher *et al.*[19] who noticed that the isotropic part of the SGS tensor is dominated by the thermodynamic pressure. This was supported by Zang *et al.*[27] who obtained indistinguishable results from LES of compressible isotropic turbulence with coefficients $C_I = 0.0066$ and 0.066.

In the present DSM simulations LESdsm and LESdsm2, SGS kinetic energy is only used in LESdsm2. No significant discrepancies are found between the results obtained from the two simulations, which show that the influence of the SGS kinetic energy on the simulated flow is negligible. This could have been expected from the above considerations, by noting that in LESdsm2 the ratio between the calculated SGS kinetic energy and the ambient pressure is about $2 \times 10^{-4}$ and that $C_I$ is about 0.01. The very small dependence on the SGS kinetic energy model is observed for flow and noise features, and is here illustrated by Figures 6 and 7 presenting the rms-values of the centerline axial velocity fluctuations and the acoustic levels for both LESdsm and LESdsm2.

## 5. Selective filtering versus eddy viscosity

The results obtained from the simulations LESsf and LESdsm are now compared to show the effects of the DSM on the turbulent jet. In LESdsm, since the mean eddy viscosity is about 40 times the molecular viscosity, one can expect the effective flow Reynolds number to be reduced from $Re_D = 4 \times 10^5$ to a value of $Re_{\nu_t} \simeq 10^4$. The discrepancies between LESsf and LESdsm should mainly result from this artificial decrease.

### 5.1 Flow field

5.1.1 Shear-layer development

As suggested by the core lengths provided in section 2.3 for LESsf anf LESdsm, the shear-layer development appears poorly affected by the use of the DSM. This is shown for instance by the streamwise variations of the shear-layer thickness and of the integral length scales presented in Figure 8, which are found to be very similar in LESsf and LESdsm.

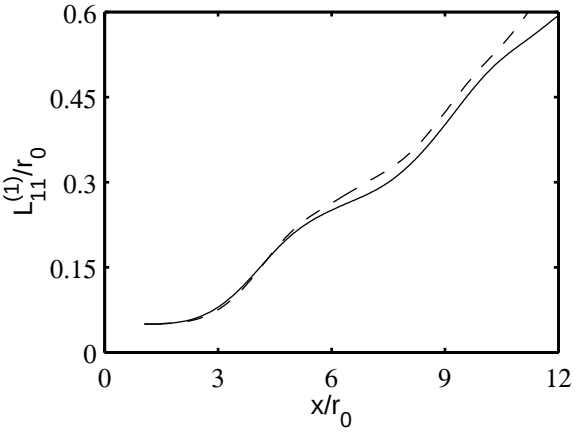


Figure 8: Profiles for $r = r_0$ of the axial length scale $L_{11}^{(1)}/r_0$. See Table 2 for the line types.

The profiles for $r = r_0$ of the rms velocity fluctuations are also in fair agreement. They have similar shapes, as in Figure 9 for the axial velocity fluctuations, with peaks reached at the same axial locations. The peak magnitudes, given in Table 3, are only slightly decreased in LESdsm. The ratios between the maxima of the axial and radial velocity fluctuations are also very close. This supports that the shear layers have similar structure in the two simulations, with and without the DSM. The shear layer development seems to be much more dependent on the excitation properties as reported in a recent paper.[21] In particular, the high values found for $v'_{rms}$ with respect to measurements[28] were observed

to be reduced when the first azimuthal modes are removed from the inflow forcing.

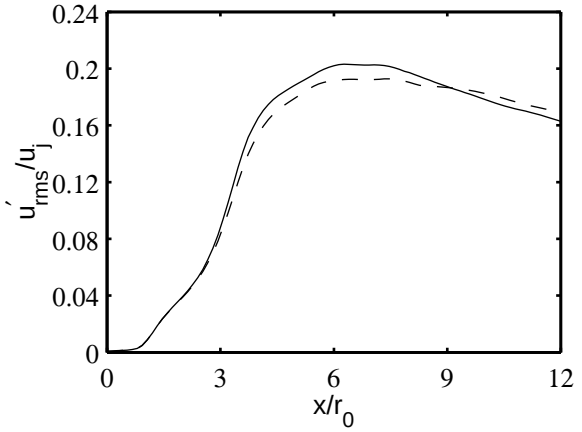


Figure 9: Profiles for $r = r_0$ of the rms-value of the fluctuating axial velocity. See Table 2 for the line types.

| | $\frac{(u'_{rms})_p}{u_j}$ | $\frac{(v'_{rms})_p}{u_j}$ | $\frac{(v'_{rms})_p}{(u'_{rms})_p}$ |
|---|---|---|---|
| LESsf | 0.203 | 0.186 | 0.92 |
| LESdsm | 0.193 | 0.175 | 0.91 |

Table 3: Rms peak values for $r = r_0$ of the fluctuating velocities $u'$ and $v'$. The subscript $p$ is used for *peak*.

To study the shear-layer turbulence, the $u'$-velocity spectra are shown for $x = 6r_0$ and $r = r_0$ in Figure 10. The spectra from LESsf and LESdsm are dominated by peaks characterized by similar Strouhal numbers and levels, indicating that the instability waves growing in the transitional shear layer are not significantly affected by the DSM. This could mostly result from the dynamic procedure which provides negligible values of coefficient $C$ in the shear layer for about $x \leq 4r_0$ as shown in Figure 1. It can be also noted that at the high flow Reynolds number $Re_D$, and even at the DSM effective $Re_{\nu_t}$, the influence of viscosity on instability waves is expected to be small.[29] Although the eddy viscosity is significant only for $x \geq 4r_0$, its dissipative effects on turbulence are yet clearly visible on the velocity spectra at $x = 6r_0$. The turbulence components with $St \geq 0.7$ are indeed reduced in LESdsm with respect to LESsf. This illustrates that the eddy viscosity affects a wide range of resolved wave numbers, located well below the filtering cut-off Strouhal number $St_c^{sf} \simeq 2.1$.

5.1.2 Jet flow development

Discrepancies between the results from LESsf and LESdsm are more apparent on the jet development downstream of the potential core. The mean flow

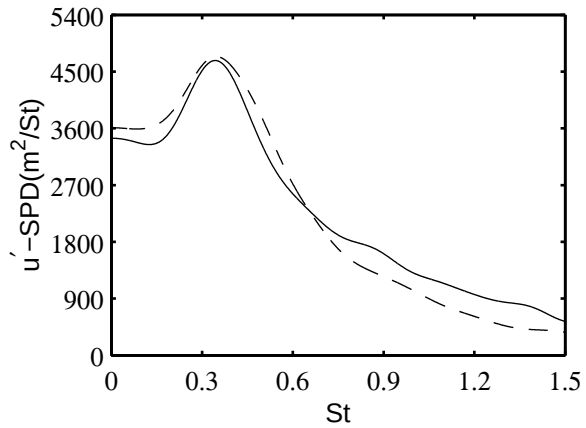


Figure 10: Spectral power densities of the $u'$-velocity for $x = 6r_0$ and $r = r_0$, as a function of Strouhal number $St = fD/u_j$. See Table 2 for the line types.

properties for instance are found to appreciably differ. The decay of the centerline axial velocity and the jet spreading are more rapid in LESdsm with the eddy-viscosity model than in LESsf. The streamwise variations of the centerline mean axial velocity are presented in Figure 11, where experimental data for two Mach $M = 0.9$ jets, at low $Re_D = 3.6 \times 10^3$ and at high $Re_D = 10^6$ Reynolds numbers respectively, are also plotted. A good agreement is observed between the velocity profile from LESsf and this measured for the high $Re_D$ jet, whereas the profile from LESdsm stands between the two experimental ones. This may indicate that the high Reynolds number $Re_D = 4 \times 10^5$ calculated from the jet inflow parameters is only preserved in the LESsf simulation. In LESdsm, the effective Reynolds number appears to be decreased. It seems intermediary from the experimental Reynolds numbers, and then corresponds well to the $Re_{\nu_t} \simeq 10^4$ estimated from the mean eddy-viscosity value $\nu_t \simeq 40\nu$.

The centerline profiles of the fluctuating velocity magnitudes are also found to differ with and without the DSM. As shown for example in Figures 4 and 6 for the fluctuating axial velocity, the amplitude peaks in LESdsm occur about one radius later than in the LESsf simulation, with slightly enhanced values. These peak values are given in Table 4 for the axial and radial velocities, and they agree fairly well with the range of corresponding measurements.[21,30]

| | $(u'_{rms})_p/u_j$ | $(v'_{rms})_p/u_j$ |
|---|---|---|
| LESsf | 0.131 | 0.118 |
| LESdsm | 0.140 | 0.120 |

Table 4: Rms peak values of the $u'$ and $v'$ velocities on the jet axis. The subscript $p$ is used for *peak*.

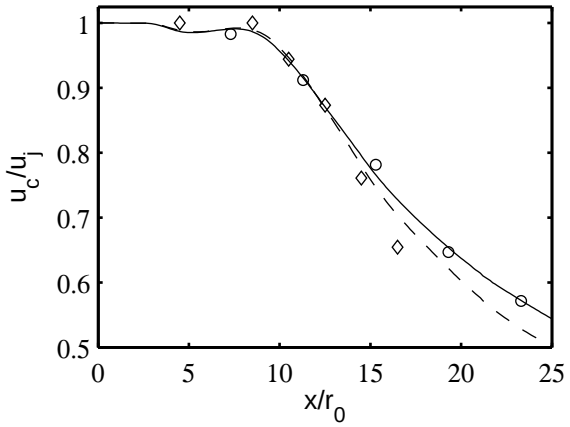


Figure 11: Profiles of the mean centerline velocity $u_c/u_j$. See Table 2 for the line types. Measurements: o Lau *et al.*[30] ($M = 0.9$, $Re_D = 10^6$), $\diamond$ Stromberg *et al.*[31] ($M = 0.9$, $Re_D = 3.6 \times 10^3$), both shifted in the axial direction for the comparison.

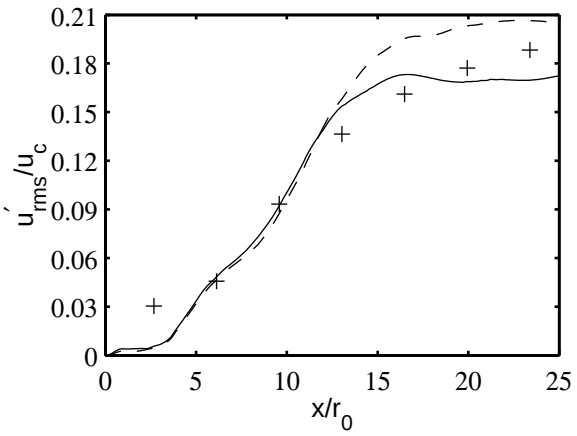


Figure 12: Centerline profiles of the turbulence intensity $u'_{rms}/u_c$. See Table 2 for the line types. + measurements of Arakeri *et al.*[33] ($M = 0.9$, $Re_D = 5 \times 10^5$), shifted in the axial direction for the comparison.

To discuss the effects of the eddy viscosity modelling on turbulence magnitude, it is more interesting to look at the turbulence intensities calculated using the local centerline velocity $u_c$. The centerline profiles of axial turbulence intensities from LESsf and LESdsm are presented in Figure 12. The self-similarity region where $u'_{rms}/u_c \simeq 0.25$ on the jet axis[32] is not observed in either of the simulations. Note that this region was shown to be still not reached in LESsf for $x = 60r_0$ in a previous study.[11] The increase of turbulence intensities in LESsf is slower than in LESdsm, and also seems to agree better with measurements for a jet at same Mach and very similar Reynolds number.[33] At this point, it should be reminded that the distance necessary for the turbulence intensities to become self-similar appears dependent on the Reynolds number. In high Reynolds number jets, the self-similarity is reached experimentally far downstream from the nozzle, at a distance of about 100 radii,[32] whereas it is observed for $x = 25r_0$ in very low $Re_D$ jets computed by Direct Numerical Simulation.[34] A faster increase in turbulence intensities should indicate a lower Reynolds number. Thus as the velocity decays, the turbulent intensities may point out that the effective Reynolds number is preserved in LESsf, but decreased in LESdsm by the eddy viscosity model.

The integral longitudinal length scales calculated on the jet axis from the axial fluctuating velocity are now presented in Figure 13. They appear to increase linearly with the downstream distance in both simulations LESsf and LESdsm. The growth rates are found to be similar, and compare to this obtained experimentally by Wygnanski and Fieldler[32] as shown in an earlier simulation using a larger grid in the axial direction.[11] It is striking to notice that the length scales are significantly larger in LESdsm than in LESsf for a given axial distance. Since the integral length scales observed in the shear layer from LESsf and LESdsm in Figure 8 are nearly the same, the discrepancies on the jet axis should mainly come from the region at the end of the potential core where the transition from shear layer to jet turbulence occurs. The eddy-viscosity DSM may thus affect appreciably the dynamics of this region.

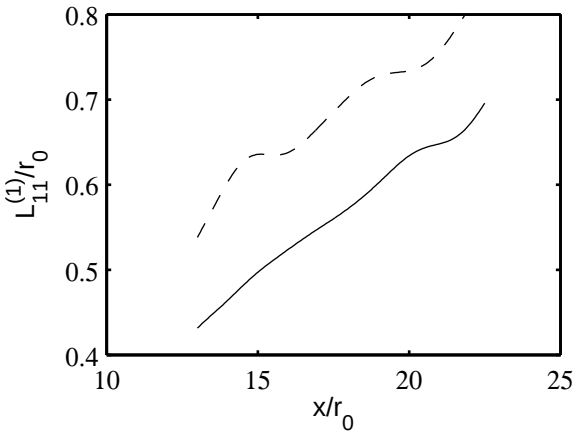


Figure 13: Centerline profiles of the axial length scale $L_{11}^{(1)}/r_0$. See Table 2 for the line types.

The $u'$-velocity spectra obtained in the developed jet for $x = 20r_0$ on the jet axis are shown in Figure 14. They are calculated from the temporal spectra using the Taylor hypothesis, as previously described in detail.[11] As expected, the spectrum from LESsf collapses in the vicinity of the filtering cut-off

wave number approximated by $k_c^{sf} = \pi/(2\Delta x)$. In LESdsm, the spectrum shape is appreciably changed with respect to LESsf and it would be more difficult to define a cut-off wave number because of the dissipative effects of the eddy viscosity on all scales. The magnitude of the higher wave numbers is reduced while this of the energy-containing lower wave numbers is enhanced in agreement with the increase in turbulence intensity. These modifications of spectrum shapes result in the description given in section 2.3 of a turbulence containing less fine scales in LESdsm than in LESsf, as for a lower Reynolds number.

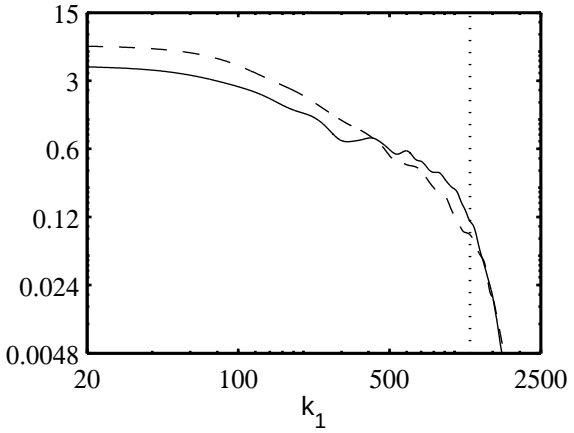


Figure 14: One-dimensional spectrum $E_u^{(1)}(k_1)$ of the $u'$ velocity for $x = 20r_0$ on the jet axis, as a function of the axial wave number $k_1$. See Table 2 for the line types, ····· filtering cut-off wave number $k_c^{sf}$.

Finally, characteristic wave numbers are reported in Table 5 for $x = 20r_0$ on the jet axis. The transverse Taylor and Kolmogorov scales are calculated using the relations for isotropic turbulence, $\lambda_g = (15L_{11}^{(1)}\nu_{ef}/u'^2_{rms})^{1/2}$ and $\eta = (L_{11}^{(1)})^{1/4}(\nu_{ef}/u'^3_{rms})^{3/4}$, where $\nu_{ef} = \nu$ in LESsf but $\nu_{ef} = \nu + \nu_t$ in LESdsm. The use of eddy viscosity in LESdsm decreases spectacularly the wave numbers associated to the Taylor and Kolmogorov scales. In particular, the Kolmogorov wave number gets closer to the range of the resolved wave numbers given by $k \leq k_c^{sf}$.

| | $1/L_{11}^{(1)}$ | $k_c^{sf}$ | $1/\lambda_g$ | $k_c^{sf}$ | $1/\eta$ |
|---|---|---|---|---|---|
| LESfs1 | 160 | 1100 | 4800 | - | 200000 |
| LESdsm1 | 130 | - | 700 | 1100 | 14000 |

Table 5: Wave numbers associated to the axial integral scale, the filtering cut-off, and the transverse Taylor and Kolmogorov scales $\lambda_g$ and $\eta$, for $x = 20r_0$ on the jet axis.

### 5.2 Acoustic field

The profiles for $r = 15r_0$ of the sound pressure levels given directly from the simulations LESsf and LESdsm are presented in Figure 15. The sound levels in LESdsm are reduced by about 1 dB with respect to LESsf for $x \leq 24r_0$, but they are increased further downstream. This change according to the direction of sound emission leads us to investigate the properties of the acoustic field in the downstream and in the sideline directions where two distinct noise components are likely to be respectively dominant.[21,24]

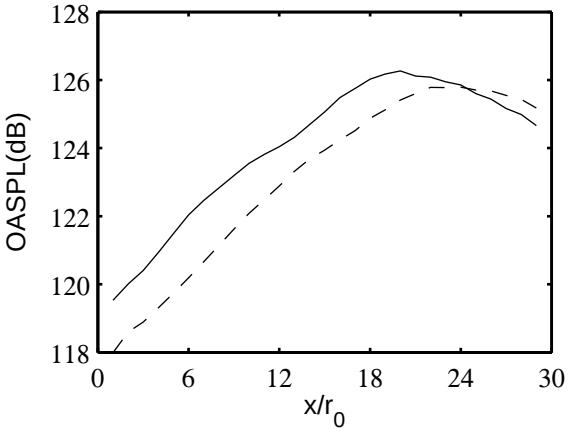


Figure 15: Overall sound pressure levels for $r = 15r_0$. See Table 2 for the line types.

Spectra and azimuthal correlation functions of the acoustic field are first calculated in the downstream direction, for $x = 29r_0$ and $r = 12r_0$ as in earlier papers.[11,21] The correlation functions from LESsf and LESdsm, not shown here, are quite similar, both displaying the high azimuthal correlation measured for angles about $\theta = 30°$ from the jet direction.[11] The mechanism generating the downstream acoustic radiation should therefore be the same in the two simulations. This is clearly demonstrated by the sound spectra presented in Figure 16, which are strongly dominated by peaks at the same Strouhal number $St \simeq 0.3$. The sound levels do not differ much, 125.2 dB in LESsf versus 126.3 dB in LESdsm, and were shown to correspond to the far-field experimental levels[11,21] for $\theta = 30°$ from the jet axis. To discuss the way the DSM may increase the downstream sound levels, remind that these levels were found to vary as the maxima of centerline turbulence intensities in recent LES.[21] The results from LESsf and LESdsm, see for instance in Table 4, conform to these observations. Thus the increase of the downstream sound levels in LESdsm may result from the higher magnitude of the velocity fluctua-

tions obtained on the jet axis just after the potential core using the DSM.

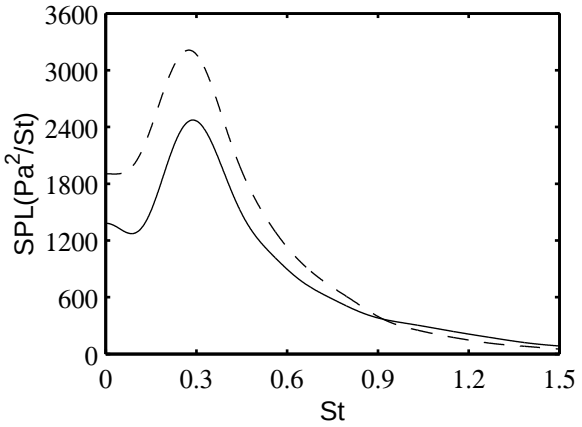


Figure 16: Sound pressure spectra as a function of Strouhal number $St = fD/u_j$ for $x = 29r_0$ and $r = 12r_0$, at an observation angle $\theta \simeq 30^o$ from the jet axis. See Table 2 for the line types.

The features of the pressure field are now investigated in the sideline direction for $x = 11r_0$ and $r = 15r_0$. As previously, the azimuthal correlation functions calculated from LESsf and LESdsm are very close, which indicates that the sound sources contributing mostly to the sideline noise in the two simulations are of same nature. The sound correlation decreases rapidly with the azimuth in accordance with experimental data.[11] It must also be noted that it is slighty enhanced in LESdsm with respect to LESsf. The effects of the subgrid modelling on the sideline noise properties are much more visible on the sound spectra presented in Figure 17. Their shapes are indeed strongly altered, with maximum for Strouhal $St \simeq 0.7$ in LESsf but for $St \simeq 0.4$ in LESdsm. The use of eddy viscosity in LESdsm thus results in the reduction of the high frequency noise components, which was already apparent in the pressure snapshots of Figure 3. The modification of the sideline spectrum shape is all the more significant because it was found to be nearly unchanged in recent LES using different parameters of inflow forcing.[21] The sound levels at the study point, 124.1 dB in LESsf versus in 122.9 dB from LESdsm, vary however as in these latter simulations, as the peak amplitudes of the fluctuating radial velocity in the shear layer, shown in Table 3. The levels are also higher by about 4 dB than expected from the far-field measurements for $\theta \simeq 75^o$ from the jet axis. This overestimation was connected to the excessive $v'_{rms}$ magnitude in the shear layer, attributed to the inflow forcing properties.[21]

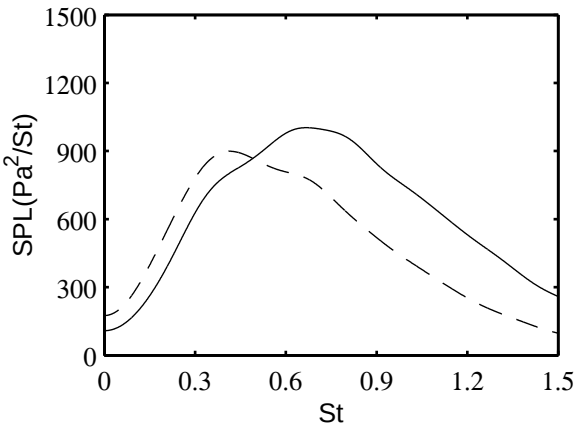


Figure 17: Sound pressure spectra for $x = 11r_0$ and $r = 15r_0$, at an observation angle $\theta \simeq 75^o$ from the jet axis. See Table 2 for the line types.

## 6. Conclusion

This paper compares the flow and sound fields calculated by Large Eddy Simulations for a subsonic, high Reynolds number circular jet using different subgrid scale modellings. The influence of the mechanism used to dissipate the turbulent kinetic energy instead of the subgrid scales is especially investigated. The jet properties are thus observed to differ appreciably when a selective filtering is used alone or in combination with the eddy-viscosity Dynamic Smagorinsky Model. The jet develops faster after the potential core with the eddy viscosity model than without, displaying for instance higher turbulence intensities and larger length scales.

These results show that the large scale features in free shear flows depend appreciably on the way the energy is dissipated. Indeed, whereas the selective filtering exerts dissipation only on the scales discretized by a small number of grid points, typically between two and four points, the eddy viscosity affects all flow scales. The eddy-viscosity model also appears to result in an artificial decrease of the effective Reynolds number of the simulated flow, which should question its use for flows where the Reynolds number is an important parameter which must be preserved.

## Acknowledgments

This work is supported by the french RRIT "Recherche Aéronautique sur le Supersonique" (Ministère de la Recherche). Computing time is supplied by the Institut du Développement et des Ressources en Informatique Scientifique (IDRIS - CNRS).

## References


[1]Lesieur, M. & Métais, O., 1996, New trends in large-eddy simulations of turbulence, *Annu. Rev. Fluid Mech.*, **28**, 45-82.

[2]Smagorinsky, J.S., 1963, General circulation experiments with the primitive equations: I. the basic experiment, *Mon. Weath. Rev.*, **91**, 99-163.

[3]Germano, M., Piomelli, U., Moin, P. & Cabot, W.H., 1991, A dynamic subgrid-scale eddy viscosity model, *Phys, Fluids A*, **3**(7), 1760-1765.

[4]Moin, P., Squires, K., Cabot, W. & Lee, S., 1991, A dynamic subgrid-scale model for compressible turbulence and scalar transport, *Phys. Fluids A*, **3**(11), 2746-2757.

[5]Lilly, D.K., 1992, A proposed modification of the Germano subgrid-scale closure method, *Phys. Fluids A*, **4**(3), 633-635.

[6]Liu, S., Meneveau, C. & Katz, J., 1994, On the properties of similarity subgrid-scale models as deduced from measurements in a turbulent jet, *J. Fluid Mech.*, **275**, 83-119.

[7]Kravchenko, A.G. & Moin, P., 1997, On the effect of numerical errors in Large Eddy Simulations of turbulent flows, *J. Comput. Physics*, **131**, 310-322.

[8]Pruett, C.D. & Adams, N.A., 2000, *A priori* analyses of three subgrid-scale models for one-parameter families of filters, *Phys. Fluids*, **12**(5), 1133-1142.

[9]Sagaut, P., 2001, Large Eddy Simulation for incompressible flows, Springer, Berlin.

[10]Domaradzki, J.A. & Adams, N.A., 2002, Direct modelling of subgrid scales of turbulence in large eddy simulation, *Journal of Turbulence*, **3** 024, 1-19.

[11]Bogey, C. & Bailly, C., 2002, Direct computation of the sound radiated by a high Reynolds number, subsonic round jet, *CEAS Workshop From CFD to CAA*, 7-8 Nov., Athens, Greece.

[12]Domaradski, J.A. & Yee, P.P., 2000, The subgrid-scale estimation model for high Reynolds number turbulence, *Phys. Fluids*, **12**(1), 193-196.

[13]Grinstein, F.F. & Karniadakis, G.E., 2002, Guest editorial of a Special section on alternative LES and hybrid RANS/LES for turbulent flows, *Journal of Fluid Engineering*, **124**, 821-822.

[14]Boris, J.P., Grinstein, F.F., Oran, E.S. & Kolbe, R.L., 1992, New insights into large eddy simulation, *Fluid Dyn. Res.*, **10**, 199-228.

[15]Lele, S.K., 1992, Compact finite difference schemes with spectral-like resolution, *J. Comput. Physics*, **103**(1), 16-42.

[16]Visbal, M.R. and Gaitonde, D.V., 1999, High-order-accurate methods for complex unsteady subsonic flows, *AIAA J.*, **37**(10), 1231-1239.

[17]Bogey, C. & Bailly, C., 2002, A family of low dispersive and low dissipative explicit schemes for computing the aerodynamic noise, *8th AIAA/CEAS Conference*, AIAA Paper 2002-2509.

[18]Visbal, M.R. & Rizzetta, D.P., 2002, Large-Eddy Simulation on curvilinear grids using compact differencing and filtering schemes, *Journal of Fluid Engineering*, **124**, 836-847.

[19]Erlebacher, G., Hussaini, M.Y., Speziale, C.G. & Zang, T.A., 1992, Toward the large-eddy simulation of compressible turbulent flows, *J. Fluid Mech.*, **238**, 155–185.

[20]Bogey, C. & Bailly, C., 2003, Selective filtering versus eddy viscosity for subgrid modelling in the LES of a high Reynolds number flow, submitted to the *ERCOFTAC Workshop Direct and Large-Eddy Simulation-5*, August 27-29, Munich, Germany.

[21]Bogey, C. & Bailly, C., 2003, LES of a high Reynolds, high subsonic jet : effects of the inflow conditions on flow and noise, *9th AIAA/CEAS Conference*, AIAA Paper 2003-3170.

[22]Vreman, B., Geurts, B. & Kuerten, H., 1995, Subgrid-modelling in LES of compressible flow, *Applied Scientific Research* , **54**, 191-203.

[23]Bogey, C. & Bailly, C., 2002, Three-dimensional non reflective boundary conditions for acoustic simulations: far-field formulation and validation test cases, *Acta Acustica*, **88**(4), 463-471.

[24]Bogey, C., Bailly, C. & Juvé, D., 2003, Noise investigation of a high subsonic, moderate Reynolds number jet using a compressible LES, *Theoret. Comput. Fluid Dynamics*, **16**(4), 273-297.

[25]Speziale, C.G., Erlebacher, G., Zang, T.A. & Hussaini, M.Y., 1988, The subgrid-scale modeling of compressible turbulence, *Phys. Fluids*, **31**(4), 940-942.

[26]Uzun, A., Blaisdell, G.A. & Lyrintzis, A.S., 2002, Recent progress towards a Large Eddy Simulation code for jet aeroacoustics, *9th AIAA/CEAS Conference*, AIAA Paper 2002-2598.

[27]Zang, T.A., Dahlburg, R.B. & Dahlburg, J.P., 1992, Direct and large-eddy simulations of three-dimensional compressible Navier-Stokes turbulence, *Phys. Fluids A*, **4**(1), 127-140.

[28]Hussain, A.K.M.F. & Husain, Z.D. , 1980, Turbulence structure in the axisymmetric free mixing layer, *AIAA Journal*, **18**(12), 1462-1469.

[29]Michalke, A., 1984, Survey on jet instability theory, *Prog. Aerospace Sci.*, **21**, 159-199.

[30]Lau, J.C., Morris, P.J. & Fisher, M.J., 1979, Measurements in subsonic and supersonic free jets using a laser velocimeter, *J. Fluid Mech.*, **93**(1), 1-27.

[31]Stromberg, J.L., McLaughlin, D.K. & Troutt, T.R., 1980, Flow field and acoustic properties of a Mach number 0.9 jet, at a low Reynolds number. *J. Sound. Vib.*, **72**(2), 159-176.

[32]Wygnanski, I. & Fiedler, H., 1969, Some measurements in the self-preserving jet, *J. Fluid Mech.*, **38**(3), 577-612.

[33]Arakeri, V.H., Krothapalli, A., Siddavaram, V., Alkislar, M.B. & Lourenco, L., 2002, Turbulence suppression in the noise producing region of a Mach=0.9 jet, *8th AIAA/CEAS Conference*, AIAA Paper 2002-2523.

[34]Freund, J.B., 2001, Noise sources in a low-Reynolds-number turbulent jet at Mach 0.9, *J. Fluid Mech.*, **438**, 277-305.